Hydrophobic Nanoparticle-Based Nanocomposite Films Using *In Situ* Ligand Exchange Layer-by-Layer Assembly and Their Nonvolatile Memory Applications

Yongmin Ko, Hyunhee Baek, Younghoon Kim, Miseon Yoon, and Jinhan Cho*

Department of Chemical and Biological Engineering, Korea University, Anam-dong, Seongbuk-gu, Seoul 136-713, Korea

ABSTRACT A robust method for preparing nanocomposite multilayers was developed to facilitate the assembly of well-defined hydrophobic nanoparticles (*i.e.*, metal and transition metal oxide NPs) with a wide range of functionalities. The resulting multilayers were stable in both organic and aqueous media and were characterized by a high NP packing density. For example, inorganic NPs (including Ag, Au, Pd, Fe_3O_4, MnO_2, $BaTiO_3$) dispersed in organic media were shown to undergo layer-by-layer assembly with amine-functionalized polymers to form nanocomposite multilayers while incurring minimal physical and chemical degradation of the inorganic NPs. In addition, the nanocomposite multilayer films formed onto flat and colloidal substrates could directly induce the adsorption of the electrostatically charged layers without the need for additional surface treatments. This approach is applicable to the preparation of electronic film devices, such as nonvolatile memory devices requiring a high memory performance (ON/OFF current ratio >10^3 and good memory stability).

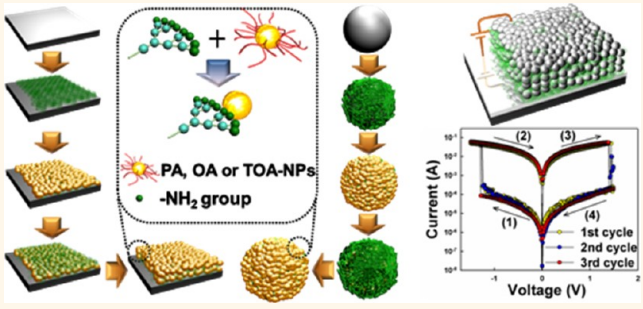

KEYWORDS: layer-by-layer assembly · multilayer · ligand exchange · nonpolar solvent · hydrophobic nanoparticles

Layer-by-layer (LbL) assembly based on complementary interactions between constituent materials is potentially the most versatile process for depositing organic/inorganic nanocomposite films with a controlled thickness, composition, and functionality onto various substrates, irrespective of the substrate size or shape.[1−26] LbL nanocomposite films have been applied to a wide range of electronic, magnetic, and optical film devices. Precise control over the relative and absolute quantities of materials during the adsorption process is central to the success of an application. The properties of the dispersed inorganic NPs themselves are also important. Functional inorganic NPs should, for most applications, be uniform in size and have a high crystallinity,[27−29] and they should adsorb densely onto a substrate.[30,31]

From a processing perspective, there is a critical need to develop a general and facile strategy for preparing LbL multilayer films using well-defined functional NPs (metal and metal oxide NPs) in organic media. LbL assembly in aqueous media is generally not directly applicable to data storage devices, such as nonvolatile memory devices, due to the evolution of undesirable leakage current arising from residual moisture. Aqueous-based LbL approaches are also not appropriate for modifying the surfaces of catalytic colloids that are used in organic dispersions in the petrochemical industry.[32] A desirable and general method for the LbL assembly of adsorption layers on substrates (large colloidal substrates, in particular) should be chemistry-independent and tolerant to a range of hydrophobic and hydrophilic moieties.

LbL-assembled polymeric/inorganic films generally rely on electrostatic attraction, hydrogen bonding, or covalent bonding

* Address correspondence to jinhan71@korea.ac.kr.

Received for review August 1, 2012 and accepted December 7, 2012.

Published online December 07, 2012
10.1021/nn3034524

between successively deposited polymer and inorganic material layers in the context of an aqueous media.[1−8,11−20] NPs synthesized in aqueous media display the relatively broad size distribution in comparison with NPs synthesized in organic media. Additionally, electrostatic repulsion among aqueous NPs with the same charge tends to limit the packing density of a NP layer to <30%.[33−35] The highest quality NPs (*i.e.*, with uniform size and high crystallinity) are synthesized using conventional hydrophobic stabilizers that have carboxylic acid or ammonium moieties (*e.g.*, oleic acid (OA), palmitic acid (PA), or tetraoctylammonium (TOA)) in organic media. The LbL assembly of hydrophobic NPs in conjunction with other materials, such as polymers, requires a phase transfer step from the nonpolar solvent to the aqueous media using selective and limited ligands that facilitate electrostatic and/or hydrogen bonding interactions.[5,8,30] Lee *et al.* reported the LbL assembly of electrostatically charged particles in a nonpolar solvent.[36] More recently, Huang and Zacharia reported that ethylene-*co*-methacrylic acid ionomers could be incorporated into polyelectrolyte complexes and thin films prepared using the LbL technique in a mixed solvent system of THF and water.[37] On the other hand, it was reported by a few research groups that amine-functionalized polymers in organic media could be LbL-assembled with dodecylamine or citrate-acid-stabilized AuNPs using high affinity between amine moieties and metal NPs (*i.e.*, LbL assembly based on ligand exchange).[21−23] Their study has focused on the preparation of polymer/metal NP nanocomposite multilayers onto flat substrates. Our research group also reported that CdSe@ZnS and Fe_3O_4 NPs modified by 2-bromo-2-methylpropionic acid (BMPA) *via* a nucleophilic substitution (NS) reaction in organic media could be LbL-assembled with a dendrimer.[9,10,32] This method proved to be non-optimal for several reasons: the BMPA ligand exchange process was difficult to apply to conventional hydrophobic metal NPs or ammonium moiety-stabilized metal oxide NPs; the resulting films were unstable in aqueous media; and hydrophilic species, such as those used in electrostatic multilayers, could not be incorporated into the hydrophobic multilayers prepared from NS-reaction-induced LbL assembly. Therefore, we hoped to design and exploit a more general, facile, and versatile strategy for incorporating a wide variety of well-defined hydrophobic NPs into functional LbL nanocomposite films in organic media, while simultaneously permitting hydrophobic and hydrophilic moieties for a wide variety of potential applications.

Here, we demonstrate that ligand-exchange-induced LbL assembly using amine-functionalized polymers can be a general approach for preparing functional nanocomposite multilayers *via* the consecutive adsorption of hydrophobic metal or metal oxide NPs onto flat or colloidal substrates (Scheme 1). The strategy is based on an *in situ* ligand exchange (ISLE) between the hydrophobic NP stabilizers and the polymer amine groups in an organic medium. This approach is advantageous in that hydrophobic NPs synthesized and/or dispersed in a nonpolar solvent can be directly used for LbL assembly without additional surface modification steps or thermal treatments. Particularly, our findings highlight that a variety of hydrophobic NPs ranging from metal to metal oxide can be LbL-assembled with amine-functionalized polymers onto flat and colloidal substrates in organic media. The adsorbed NPs exhibited a high layer density of approximately 60% per layer. Electrostatic multilayers could be adsorbed onto hydrophobic NP multilayer-coated flat or colloidal substrates *via* successive deposition processes.

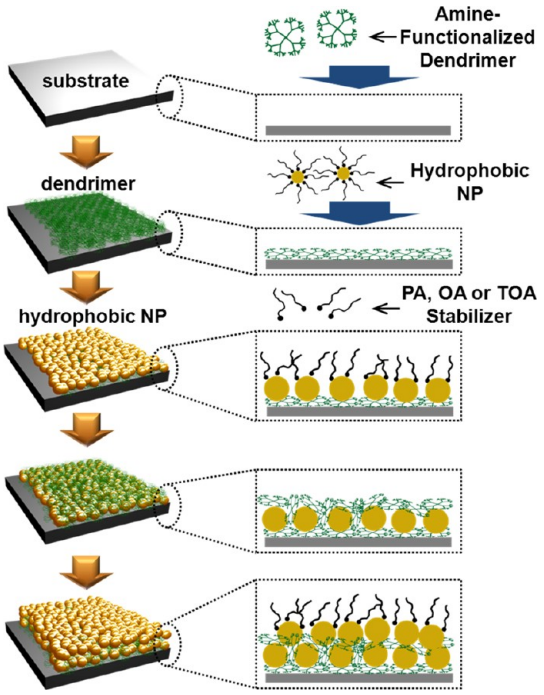

Scheme 1. Schematic diagram showing the preparation of (dendrimer/hydrophobic NP)$_n$ multilayers using ISLE-induced LbL assembly approach in organic media.

It was also demonstrated that the ISLE-induced LbL assembly method for preparing nanocomposite films could be applied to the preparation of a nonvolatile resistive switching memory device for mobile electronics. The hydrophobic multilayer device yielded an ON/OFF current ratio of $>10^3$, a good retention stability, and an overall performance that was superior to a similar hydrophilic multilayer device and comparable to a conventional transition metal oxide device fabricated using a vacuum deposition process with high temperature annealing (>200 °C). This strategy may be useful for preparing high-performance catalytic films, energy harvesting devices, functional colloids, and electronic devices.

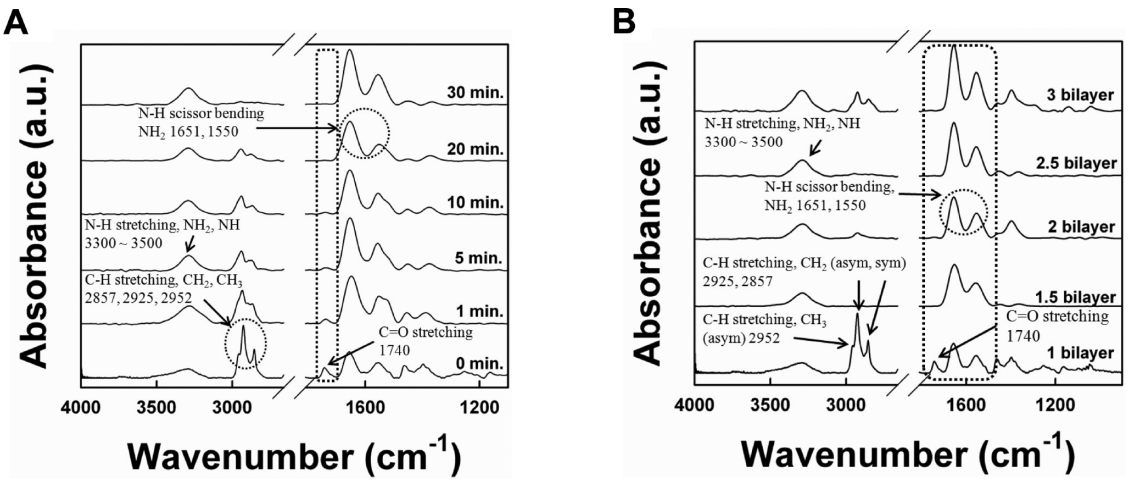

Figure 1. ATR-FTIR spectra of LbL film as a function of (A) deposition time of the dendrimer layer onto PA-AgNP-coated films, and (B) the number (*n*) of (dendrimer/PA-AgNP)$_n$ multilayers.

RESULTS AND DISCUSSION

Adsorption Behavior for the Formation of ISLE-LbL Multilayers. Ag nanoparticles stabilized by PA (PA-AgNP) with a diameter of approximately 5 nm were prepared in toluene.[38] As previously mentioned, these hydrophobic stabilizers (OA, PA, or TOA) in a nonpolar solvent produce large quantities of a variety of metal (*i.e.*, Ag, Au, or Pd) and metal oxide (*i.e.*, Fe_3O_4, MnO_2, or $BaTiO_3$) NPs with uniform sizes and in high concentrations. PA-AgNP was deposited directly onto planar substrates coated with poly(amidoamine) dendrimer or poly(ethylene imine) (PEI). Although the PA ligands onto an AgNP surface have no affinity for the dendrimer, the carboxylic acid groups of PA, loosely bound to the AgNP surface, can easily be replaced by the amine moieties of the dendrimer *via* ligand exchange during deposition. As an electron donor, the $-NH_2$ group preferentially bound to metal or transition metal oxide NPs *via* a coordination bond.[39] More specifically, when PA-AgNPs were deposited onto the dendrimer-coated surface, the PA stabilizers bound to the bottom surface of AgNPs were replaced by amine groups of dendrimer. In this case, the top surface of PA-AgNPs unbound to the dendrimer layer was still stabilized with the remaining PA ligands. However, the successive deposition of a new dendrimer layer onto the top surfaces of PA-AgNPs completed the replacement of the remaining PA stabilizers with amine-functionalized dendrimers. Alternate deposition of the PA-AgNPs and dendrimers thereby yielded a coordinatively cross-linked multilayer (Scheme 1).

The presence of residual PA ligand in the ISLE-induced LbL-grown dendrimer/PA-AgNP multilayers was examined using Fourier transform infrared (FTIR) spectroscopy in attenuated total reflection (ATR) mode (Figure 1). The ATR-FTIR spectra of the PA-AgNP and the dendrimer displayed absorption peaks originating from the carbonyl (C═O) stretching vibration of a carboxylic acid group at 1740 cm^{-1} and N−H bending vibration of amine groups ($-NH_2$) at 1651 and 1550 cm^{-1}, respectively (Figure 1A).[40,41] Therefore, two noticeable absorption peaks deriving from the C═O stretching and −N−H bending were observed in the dendrimer/PA-AgNP film. As the dendrimer layer was further adsorbed onto the PA-AgNP-coated film as a function of deposition time, the absorption peak intensity of the C═O stretching at 1740 cm^{-1} significantly decreased at 5 min and almost completely disappeared after 30 min (Figure 1A and Figure S1). In contrast, the intensity of the $-NH_2$ group peak increased over the same period. The alternating deposition of the dendrimer and the PA-AgNP produced inversely correlated changes in the peak intensities of the N−H bending and C═O stretching frequencies (Figure 1B). As mentioned earlier, the AgNP layers (*e.g.*, 1.5 and 2.5 bilayered films) buried between adjacent dendrimer layers did not contain the PA ligands. In the case of 1, 2, and 3 bilayered films, PA ligands were present on the top surface of the outermost AgNP layer. As the bilayer number increased, the peak intensity corresponding to the carbonyl groups present on the top surface of the outermost PA-AgNP layer decreased significantly compared to the peak intensity corresponding to the NH_2 groups of the dendrimer layers. The carbonyl group peak intensity was barely detectable after two bilayer deposition steps due to concentration effects.

These results evidently indicate that the PA ligands bound to AgNP were exchanged with dendrimer chains. The adsorption kinetics of the PA-AgNP onto the dendrimer layer and the dendrimer onto the PA-AgNP layer were examined using quartz crystal microgravimetry (QCM). The quantities of dendrimers adsorbed onto the AgNP layer and AgNP adsorbed onto the dendrimer layer reached a plateau after 30 and 60 min, respectively (Figure 2). The deposition time required to reach saturating amounts of PA-AgNPs

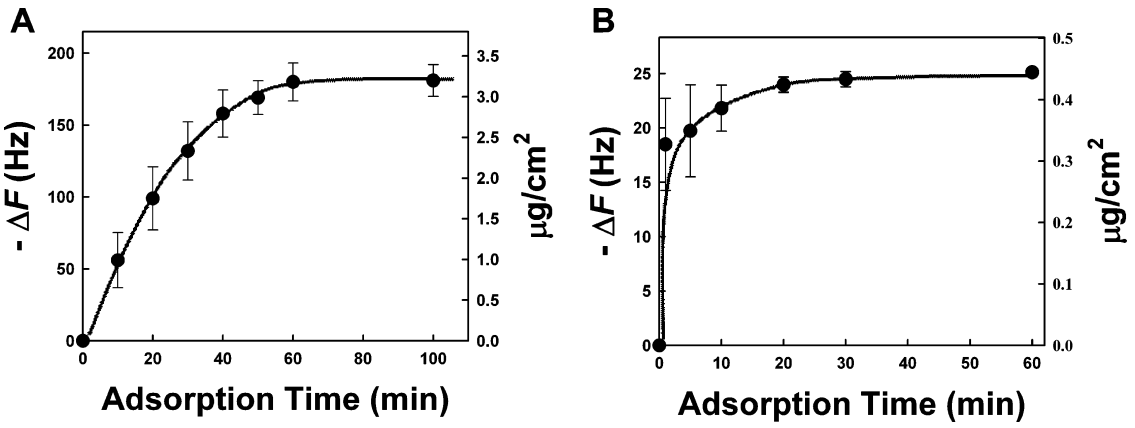

Figure 2. Adsorption isotherm behavior of (A) a PA-AgNP layer onto a dendrimer layer, and (B) a dendrimer layer onto a (dendrimer/PA-AgNP)$_1$-coated QCM electrode. Saturated quantities of PA-AgNP and dendrimer were observed for adsorption times of 60 and 30 min, respectively. The solid lines were drawn as a guide for the eye.

decreased with increasing solution concentration (see the Supporting Information, Figure S2). This adsorption behavior suggested that the dendrimer and the PA-AgNP remained stable during the LbL assembly, effectively eliminating the nonspecific adsorption of additional dendrimer and PA-AgNP. Otherwise, AgNP aggregation would cause a continuous increase in mass with increasing adsorption time.

On the basis of these results, the growth of multilayers was quantitatively monitored using QCM. Figure 3A shows the frequency changes, $-\Delta F$, and the mass changes in the adsorbed dendrimer and PA-AgNP that resulted from an increasing layer number. The mass changes were calculated from the frequency changes of the dendrimer and the PA-AgNP layers adsorbed on the crystal surface, assuming that the layers were rigid, evenly distributed, and sufficiently thin to satisfy Sauerbrey equation (see Methods). Alternating the deposition of the dendrimer and the PA-AgNP resulted in $-\Delta F$ of 22 $\pm$ 6 (Δm of ~388 ng·cm^{-2}) and 180 $\pm$ 9 Hz (Δm of ~3180 ng·cm^{-2}) per layer, respectively. The QCM measurements agreed with the thermogravimetric analysis (TGA) within experimental error range (see the Supporting Information, Figure S3). That is, the mass ratio of the dendrimer to the PA-AgNP calculated from QCM analysis was 0.112:0.888. On the other hand, the mass ratio of the organic components (dendrimer and PA ligands) to the AgNPs obtained from TGA measurement was measured to be 0.132:0.868 by TGA measurement.

Considering that the diameter and the density of the AgNP used were approximately 5 nm and 10.5 g·cm^{-3}, respectively, the number density of the AgNP in each AgNP layer was calculated to be approximately 4.62 $\times$ 10^{12} cm^{-2} (by QCM analysis), corresponding to a packing density of about 60% in single NP layered volume or 54% in a cubic volume. This value was close to the maximum packing density, corresponding to a random close packing density of ~64% in a cubic volume,[42−44] for identical solid spheres. If there is no nanopore within multilayers and the packing density of AgNPs is about 54% in cubic form, the volume packing density of dendrimers in cubic form is calculated to be about 46%. However, if the density of dendrimer is assumed to be the bulk dendrimer density of 1.3 g·cm^{-3}, and the packing density of dendrimers is further calculated using QCM or TGA measurement, their packing density is increased up to about 49.6 or 54% in cubic form, respectively. The discrepancy of these experimental values is mainly caused by a number of assumptions (*i.e.*, the respective size and density of AgNP and dendrimer, the shape of adsorbed dendrimer, the amount of residual solvent within dendrimer layers, *etc.*). Although poly(amidoamine) dendrimers employed for our study display the globular shape in solution, they are highly compressed along the surface normal, and flattened along the surface plane within self-assembled films (see Supporting Information, Figure S5).[45] Therefore, in our system, we focused on the packing density of a single AgNP layer excluding a dendrimer layer. Additionally, the packing density of a single AgNP layer is directly related to the adsorbed amount of inorganic NPs.

The high packing densities of hydrophobic NPs shown in our system have not been easily achieved using electrostatic LbL assembly approaches (see the Supporting Information, Figure S4). The dense packing of the PA-AgNP was confirmed using high-resolution transmission electron microscopy (HR-TEM) (Figure 3B). Figure 3C demonstrates that the thickness of the dendrimer/PA-AgNP multilayer thin films varied linearly with the number of layers. The measured film thickness almost coincided with the ideal film thickness (*i.e.*, a 5 nm sized PA-AgNP and dendrimer layer thickness of approximately 1 nm per bilayer). The surface roughness of the (dendrimer/PA-AgNP)$_n$ films was measured to be approximately 1.1 nm (Figure 3D).

We next investigated the applicability of the ISLE approach to the LbL assembly with an amine-functionalized dendrimer of OA-Fe_3O_4 NPs (7 nm in diameter)[46] and TOA-Au_{NP} (6 nm)[47,48] synthesized in toluene. ATR-FTIR

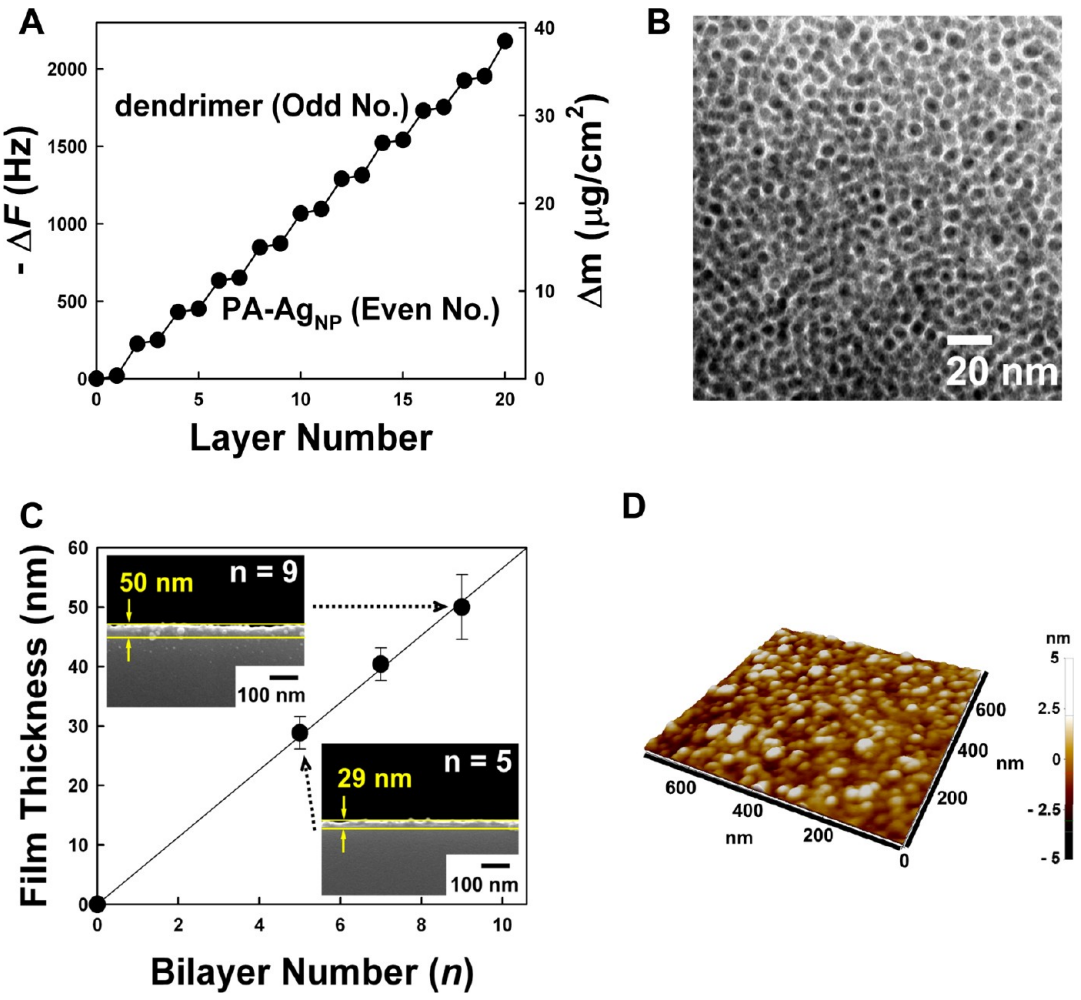

Figure 3. (A) QCM data of (dendrimer/PA-AgNP)$_n$ as a function of layer number. (B) HR-TEM image of a 5 nm sized PA-AgNP single layer adsorbed onto dendrimer-coated TEM grids. The PA-AgNP layer showed a packing density of approximately 60%. (C) Film thickness of (dendrimer/PA-AgNP)$_n$ as a function of the layer number and bilayer number. The inset shows the cross-sectional scanning electron microscopy (SEM) images of the films. (D) AFM image of (dendrimer/PA-AgNP)$_n$ multilayers. The root-mean-square (rms) surface roughness of the film was measured to be about 1.1 nm of (dendrimer/PA-AgNP)$_n$, where n = 5 and 9.

spectra revealed the successful formation of multilayer films *via* the mechanism described above (Figure 4). In the case of the dendrimer/OA-Fe_3O_4 multilayers, the C═O stretching vibration at 1740 cm^{-1} corresponding to the OA ligands disappeared in the dendrimer/OA-Fe_3O_4 multilayers as the dendrimer was adsorbed onto the OA-Fe_3O_4 layer-coated films, similar to the trend observed for the dendrimer/PA-AgNP multilayers. Although the $-COO^-$ group in the OA acted either as a chelated ligand, binding to Fe *via* two O atoms, or as a monodentate molecule, linking to an Fe atom *via* only one O atom,[39] the OA ligands were almost completely replaced by dendrimer. Deposition of the dendrimer onto the TOA-AuNP layer could be monitored by the development of a strong C−H stretch at 1651 and 1550 cm^{-1}. The TOA ammonium ions bound to the AuNPs were easily replaced by the primary amine group from the dendrimer, which bound to the Au centers in the AuNPs with a high binding energy.[49,50] This approach is advantageous relative to LbL films that rely on thiol-containing organics because the chemistry of the metal NP surfaces, including any catalytic properties, may be preserved by avoiding strong covalent bonds.[51] It should be also noted that other amine-functionalized polymers such as PEI could be directly LbL-assembled with a variety of metal oxide NPs as well as metal NPs *via* ligand exchange between amine moieties and hydrophobic stabilizers (*i.e.*, OA, PA, or TOA) of NPs (see Supporting Information, Figure S6).

Solution Stability of ISLE Multilayers. The versatility of our approach was tested in a qualitative investigation of the vertical growth of LbL nanocomposite multilayers prepared with a variety of well-defined metal NPs (5 nm PA-AgNPs, 6 nm TOA-AuNPs, and 6 nm TOA-PdNP[48]) or transition metal oxides (7 nm OA-Fe_3O_4, 6 nm TOA-MnO_2,[52] and 7 nm $BaTiO_3$[53]). A linear increase in the UV−vis absorption intensity of the (dendrimer/

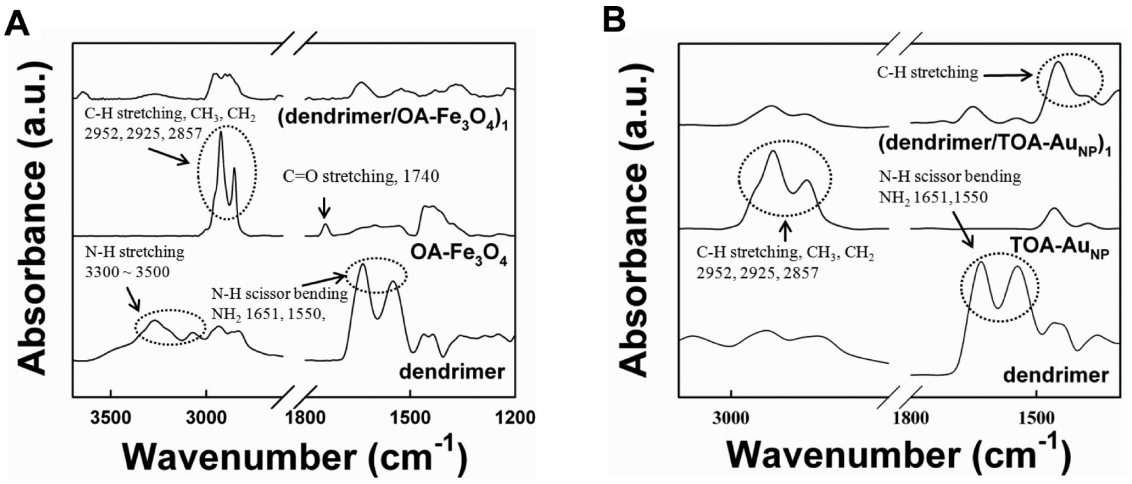

Figure 4. (A) ATR-FTIR spectra of dendrimer, OA-Fe_3O_4, and dendrimer/OA-Fe_3O_4 films. (B) ATR-FTIR spectra of dendrimer, TOA-AuNP, and dendrimer/TOA-AuNP films.

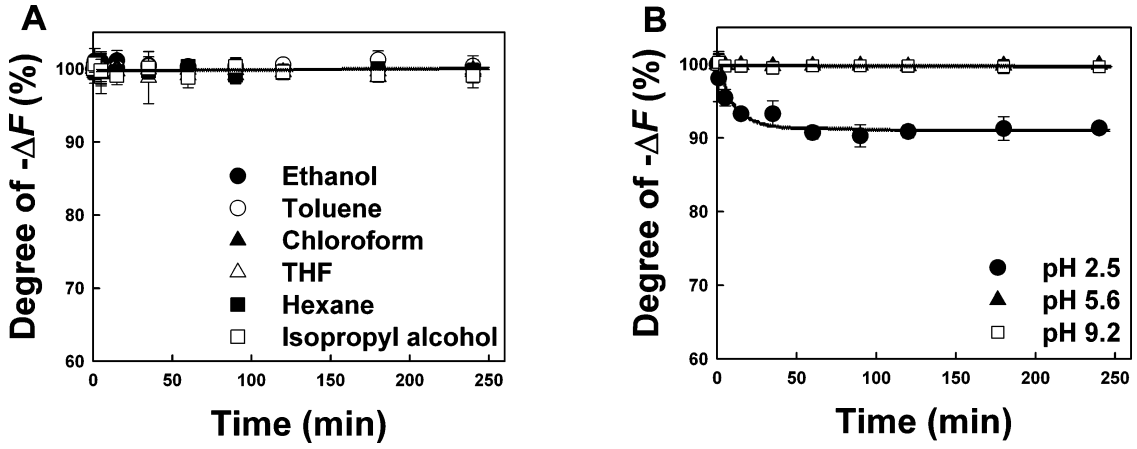

Figure 5. Values of $-\Delta F$ (%) measured for the dendrimer/PA-AgNP multilayers as a function of (A) immersion time in toluene, THF, chloroform, hexane, and isopropyl alcohol solvents and (B) immersion time in aqueous solutions of pH 2.5, 5.6, and 9.2.

hydrophobic NP)$_n$ multilayers with increasing bilayer number (n) confirmed the LbL growth *via in situ* ligand exchange from the PA, OA, or TOA ligands to the dendrimer (see Supporting Information, Figure S7). Furthermore, we observed that ISLE-based LbL films generally exhibited a high stability in a variety of organic media (Figure 5A) and in aqueous solutions. These films did show a 10% loss in mass in a pH 2.5 aqueous solution (Figure 5B), possibly due to an increase in the electrostatic repulsion among the dendrimer chains.

The pK_a (*i.e.*, the pH value at which 50% of a polymer's functional groups are ionized) of the amine-functionalized dendrimers was 9.0, and the amino groups are expected to be fully protonated at low pH.[54] Despite the partial mass loss, the films remained otherwise stable. In light of these results, the ISLE approach may potentially be useful for the preparation of electrostatic LbL multilayers composed of positively charged poly(allylamine hydrochloride) and negatively charged enzymes (*i.e.*, catalase) by deposition at pH 9 (see Supporting Information, Figure S8).

ISLE-LbL Multilayers onto Colloidal Substrates. Given these results, we prepared functional colloids based on ISLE-induced LbL assembly. Hydrophobic NPs (PA-AgNPs and OA-Fe_3O_4) were deposited onto a dendrimer-coated silica colloid with a diameter of approximately 580 nm. A dendrimer was subsequently adsorbed onto the hydrophobic NP-coated colloids. As shown in Figure 6, densely and uniformly coated AgNP or Fe_3O_4 layers were successfully deposited onto colloids in an organic solvent without inducing colloidal aggregation. The functional colloids coated with the (dendrimer/PA-AgNP)$_5$ or (dendrimer/7 nm sized OA-Fe_3O_4)$_5$ multilayers were 635 or 667 nm in diameter, respectively. The ISLE-induced LbL multilayer-coated colloids were well-dispersed in a variety of organic solvent media, including toluene, hexane, chloroform, tetrahydrofuran, or ethanol.

Fabrication of Nonvolatile Memory Devices Using ISLE-LbL Multilayers. On the basis of these results, we fabricated nonvolatile memory devices[55−61] using about 25 nm thick dendrimer/OA-Fe_3O_4 multilayers with

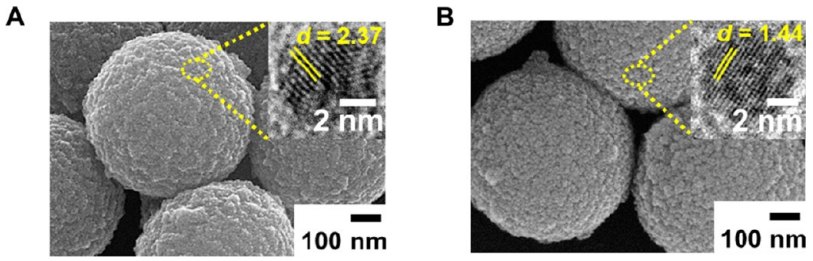

Figure 6. SEM images of SiO_2 colloids coated with (A) (dendrimer/PA-AgNP)$_5$ and (B) (dendrimer/OA-Fe_3O_4)$_5$ multilayers. The insets indicate the HR-TEM images of PA-AgNP and OA-Fe_3O_4 NP.

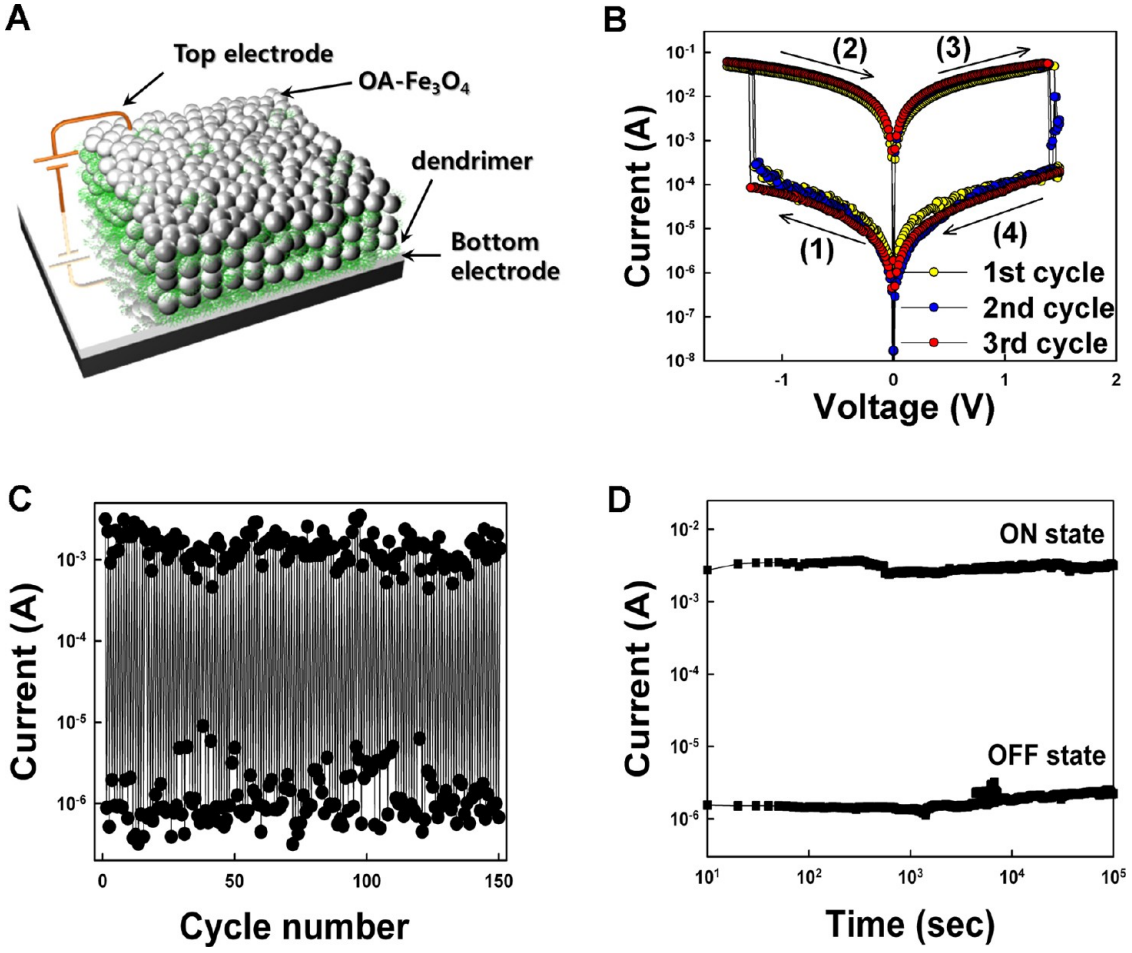

Figure 7. (A) Schematic diagram of a nonvolatile memory device based on ISLE-induced LbL-assembled dendrimer/OA-Fe_3O_4 multilayers. (B) $I-V$ curves of the (dendrimer/OA-Fe_3O_4)$_3$ film device obtained from the repeated operation cycles in the same top electrode. (C) Cycling and (D) retention time tests of a 3 bilayered device measured at a switching speed of 100 ns at a reading voltage of 0.1 V.

superparamagnetic properties (see Supporting Information, Figure S9). These multilayers were sandwiched between platinum bottom and tungsten top electrodes with about 50 μm diameter (Figure 7A). As shown in Figure 7B, these nanocomposite devices exhibited bipolar resistive switching properties, depending on the voltage polarity when the voltage was swept from 0 to -1.5 V and then back to $+1.5$ V with a limited current compliance up to 100 mA. The high-current state (the "ON" state) that formed after the initial electroforming stage (for a conductive path within multilayers) was suddenly converted to a low-current state (RESET process for the "OFF" state) at $+1.5$ V when the reverse voltage polarity was applied to the (dendrimer/OA-Fe_3O_4)$_3$ multilayered devices. This low-current state (the OFF state) was maintained from $+1.5$ to -1.4 V and converted to the high-current state at -1.4 V (SET process for the ON state). As a result, these devices exhibited a relatively high ON/OFF current ratio of $\sim 10^3$. The memory performance of these devices was obtained without thermal treatment to improve the electrical performance of transition metal oxide films.

In contrast, the film devices based on aqueous anionic Fe_3O_4 NPs[62] (see Supporting Information, Figure S10) and a cationic polyelectrolyte displayed a low ON/OFF current ratio below 10 due to the formation of a relatively high OFF current state (*i.e.*, leakage current) and low packing density of aqueous Fe_3O_4 NPs (see Supporting Information, Figure S11).

To further investigate the stability of the resistive switching properties in OA-Fe_3O_4 NP-based multilayer devices, cycling and retention time tests were performed on 3 bilayered dendrimer/OA-Fe_3O_4 film devices to determine their electrical stability in the ON and OFF states using a reading voltage of +0.1 V (Figure 7C,D). Additionally, stable ON and OFF states were maintained during repeated tests of approximately 150 cycles and a test period of 10^5 s in air. These results imply that resistive switching nonvolatile memory devices composed of ISLE-induced LbL multilayer devices exhibit good electrical stability. To comprehend the conducting behavior of the dendrimer/OA-Fe_3O_4 film devices, the $I-V$ characteristics during negative voltage sweep were plotted on a log−log scale (see Supporting Information, Figure S12). The $I-V$ relationship in the ON state exhibited ohmic conduction behavior with a slope of ~1.01, which indicates the formation of conductive paths in the device during the SET process. In contrast, the conduction behavior in the OFF state followed the trap-controlled space-charge-limited conduction (SCLC) consisting of an ohmic region ($I \propto V$) at a low negative voltage, a transition region ($I \propto V^2$) from ohmic to SCLC transport, and a region of the sharp current increase.

The switching mechanism based on the Memristive model[56,57] can be proposed for the resistive switching behavior in ILSE-induced (dendrimer/OA-Fe_3O_4)$_n$ films. The positively charged carriers (*i.e.*, the Fe ions) in the Fe_3O_4 lattices are repelled or attracted from the top electrode according to the electric field and can drift as a result of tunneling through a thin residual region (*i.e.*, undoped charge carrier region within 7 nm sized Fe_3O_4 and dendrimer layers of about 1 nm thickness per bilayer). This result has a significant effect on the electronic barrier to the electron transport at the interface between the electrode and multilayers. Therefore, a negative voltage applied to the top electrode attracts positively charged carriers in the Fe_3O_4 lattices. These charges drift in the electric field through the most favorable diffusion paths to form channels of high electrical conductivity. Once more conductance channels penetrate the electronic barrier, the device is switched ON, producing a symmetric $I-V$ curve that is the result of tunneling through a thin insulating barrier. However, when a voltage with a reverse polarity is applied to the top electrode, the positively charged carriers in the conducting channel are repelled from the top interface, and the original electronic barrier is recovered. Recently, Kim *et al.* suggested that both the time-dependent capacitance and the time-dependent resistance in the Memristive model arose from Fe^{2+} and Fe^{3+} having different mobilities in the nanoparticle lattices.[63] When a voltage with a reverse polarity was applied to the top electrode, the charged carriers were repelled from the top interface (low-current state). Considering that a range of transition metal oxide such as TiO_2,[57] Fe_3O_4,[63] or ZnO[64] can exhibit the resistive switching behavior according to externally applied voltage and the ISLE-induced LbL-assembly can provide an insight into the preparation of metal oxide NP-based multilayer films in organic media, we believe that our approach is effective for designing the nanocomposite memory devices with desired material components and functionalities.

CONCLUSION

In conclusion, we successfully prepared LbL multilayer films based on a variety of hydrophobic metal or transition metal oxide NPs using an ISLE reaction between hydrophobic ligands loosely bound to NPs and amine-functionalized dendrimers in organic solvent. This strategy allowed the formation of nanocomposite multilayer films with a maximal NP packing density of approximately 60% and excellent solvent stability due to the formation of relatively strong specific bonding between metal (or transition metal oxide) NPs and the dendrimer. Additionally, our approach could directly induce the deposition of electrostatic LbL-assembled enzymes onto hydrophobic NP-based multilayers without the need for additional surface modification steps. Furthermore, we demonstrated that the polymer/inorganic NP multilayers prepared from an ILSE-induced LbL assembly could be effectively used for electronic devices such as nonvolatile memory devices. In a future publication, we will show that high-performance energy harvesting film devices using $BaTiO_3$ and catalytic colloids using noble metal NPs and enzymes can be readily prepared using our approach.

METHODS

Synthesis of PA- and OA-AgNPs. PA or OA (2.8 g, Aldrich, St. Louis, MO, USA) was dissolved in triethylamine (40 mL, Aldrich) followed by adding $AgNO_3$ (1.8 g, Aldrich). After 10 min of stirring, the solution turned into a white slurry which was refluxed at 80 °C for 2 h. The synthesized AgNPs were purified twice by adding acetone (40 mL) followed by centrifugation at 3500 rpm for 5 min. These AgNPs were dried under vacuum and then dispersed in toluene.

Synthesis of TOA-AuNPs and PdNPs. TOA-stabilized AuNPs and PdNPs of about 6 nm were synthesized in toluene and added to a 25 mM solution of TOA bromide in toluene (80 mL, Fluka). The transfer of the metal salt to the toluene phase could be clearly seen within a few seconds. A 0.4 M solution of freshly prepared $NaBH_4$ (25 mL, Aldrich) was added to the stirred mixture, which

caused an immediate reduction. After 30 min, the two phases were separated, and the toluene phase was subsequently washed with 0.1 M H_2SO_4, 0.1 M NaOH, and H_2O (three times).

Synthesis of OA-Fe_3O_4. OA-stabilized Fe_3O_4 of about 7 nm was synthesized in toluene as reported previously by Sun *et al.*[46] $Fe(acac)_3$ (2 mmol), 1,2-hexadecanediol (10 mmol), OA (5 mmol), oleylamine (6 mmol), and benzyl ether (20 mL) were mixed and stirred under a flow of nitrogen. The mixture was heated to 200 °C for 2 h and heated to reflux (about 300 °C) for 1 h under a blanket of nitrogen. The black-colored mixture was cooled to room temperature by removing the heat source. Ethanol (40 mL) was added to the mixture under ambient conditions, and a black material was precipitated and separated *via* centrifugation. The black product was dissolved in hexane in the presence of OA (0.05 mL) and oleyamine (0.05 mL). Centrifugation (6000 rpm, 10 min) was applied to remove any undispersed residue. A black-brown hexane dispersion of 7 nm Fe_3O_4 nanoparticles was produced.

Synthesis of TOA-MnO_2. TOA-MnO_2 solution was synthesized using a two-phase extraction process shown in TOA-AuNP and TOA-PdNP. First, an aqueous solution of $KMnO_4$ (5 mL, 10 mM, Aldrich) and 50 mL of toluene were mixed together in a 100 mL separating funnel. Then, 25 mg of TOA (Fluka), a phase transfer reagent, was introduced and shaken vigorously. As a consequence, MnO_4^- was transferred from the aqueous phase the organic layer, leaving behind a colorless aqueous solution. After adding 5 mg of tetrabutylammonium borohydride ($TBABH_4$) to this organic phase and shaking vigorously, the purple color of the solution became brown, which indicated evolution of MnO_2 NPs in toluene. After 30 min, the water phase was removed and then purified twice by pH 5.8 aqueous media.

Synthesis of OA-$BaTiO_3$. Barium titanium glycolate was first prepared for OA-$BaTiO_3$ NPs. In a 250 mL round-bottom flask, 78 mmol of barium oxide fine powder (97%, Aldrich) was added to 60 mL of ethylene glycol. The reaction mixture was stirred vigorously until the added fine powder was dissolved and then diluted with 80 mL of 2-propanol. Titanium isopropoxide (18 mL, 97%, Aldrich) was then added to the reaction mixture with vigorous stirring for 1 h. The product precipitated from solution was collected by centrifugation, washed with 2-propanol, and dried in a vacuum.

After synthesized barium titanium glycolate, OA-$BaTiO_3$ NPs were prepared as follows in a 250 mL three-neck flask, a mixture of 50 mL of diphenyl ether, and 5–45 mmol OA was dried at 120 °C for 1 h under an argon atmosphere with vigorous stirring. After the mixture was cooled to 100 °C, 5 mmol barium titanate glycolate was added under vigorous stirring until the added precursors dissolved. A 1.8 g aqueous solution containing 30% hydrogen peroxide was then injected into the mixture slowly. The mixture was maintained in a closed system at 100 °C and stirred under mild reflux with water for 48 h under an inverse micelle condition. After the reaction mixture was cooled to room temperature, the product was readily precipitated by adding excess ethanol to the reaction mixture. The resulting precipitate was isolated by centrifugation and repeatedly washed with ethanol to remove the surfactant residuals.

Buildup of Multilayers. A toluene or hexane dispersion of hydrophobic NPs and an ethanol solution of the dendrimer were prepared at concentrations of 5 and 1 mg·mL^{-1}, respectively. Prior to LbL assembly, the quartz or silicon substrates were cleaned with an RCA solution ($H_2O/NH_3/H_2O_2$ 5:1:1 v/v/v). The substrates were dipped into the dendrimer solution for 10 min, washed twice with ethanol, and dried under a gentle nitrogen stream. The dendrimer-coated substrates were dipped into a hydrophobic NP solution for 60 min, followed by washing with toluene and drying with nitrogen. The substrates were then dipped into the dendrimer solution for another 30 min. The dipping cycles were repeated until the desired number of layers had been obtained.

For the successive deposition of electrostatic multilayers onto ISLE-induced LbL multilayers, positively charged poly(allylamine hydrochloride) (PAH) (M_w = 70 000, Aldrich) and negatively charged catalase (CAT) (from bovine liver, Aldrich) were alternately deposited onto (dendrimer/PA-AgNP)$_n$ multilayers. The PAH (pH 9) and CAT solutions (pH 9) used for all experiments were adjusted to 1 mg·mL^{-1}. Deionized water was used as washing solution, and all deposition processes were identical to those mentioned above.

The (dendrimer/hydrophobic NP)$_n$ multilayer-coated silica colloids were prepared as follows: 100 μL of a concentrated dispersion (6.4 wt %) of anionic 600 nm SiO_2 colloids was diluted to 0.5 mL with deionized water. After centrifugation of the colloidal solution (8000 rpm, 5 min), the supernatant water was removed, the 1 mg·mL^{-1} dendrimer ethanol solution was added to the colloids, and the solution was subject to ultrasonication. Excess dendrimer was removed by three centrifugation (8000 rpm, 5 min)/wash cycles. A 0.5 mL volume of PA-AgNP (or OA-Fe_3O_4) (5 mg·mL^{-1}) in toluene was added to prepare multilayers on the dendrimer-coated SiO_2 colloids. The excess NP was removed after deposition for 10 min by three centrifugation steps, as described above. A 0.5 mL aliquot of the 1 mg·mL^{-1} dendrimer solution in toluene (or ethanol) was then deposited onto the hydrophobic NP-coated colloids under the same conditions. The above process was repeated until the desired number of layers was deposited on the colloidal silica.

UV–Vis Spectroscopy. UV–vis spectra of dendrimer/hydrophobic NP multilayers on quartz glass were collected with a Perkin-Elmer Lambda 35 UV–vis spectrometer.

Quartz Crystal Microgravimetry (QCM) Measurements. A QCM device (QCM200, SRS) was used to examine the mass of the material deposited after each adsorption step. The resonance frequency of the QCM electrodes was approximately 5 MHz. The adsorbed mass of dendrimer and hydrophobic NPs, Δm, was calculated from the change in QCM frequency, ΔF, using the Sauerbrey equation:

$$\Delta F(\mathrm{Hz}) = -\frac{2F_0^2}{A\sqrt{\rho_q \mu_q}} \cdot \Delta m$$

Here, F_0 (~5 MHz) is the fundamental resonance frequency of the crystal, A is the electrode area, and ρ_q (~2.65 g·cm^{-2}) and μ_q (~2.95 × 10^{11} g·cm^{-2}·s^{-2}) are the shear modulus and density of quartz, respectively. This equation can be simplified as follows:

$$\Delta F(\mathrm{Hz}) = -56.6 \times \Delta m_A$$

where Δm_A is the mass change per quartz crystal unit area in μg·cm^{-2}.

Measurement of Film Stability. To investigate the film stability in water at various pH values, as well as organic media, nine identical samples composed of (dendrimer/PA-AgNP)$_5$ multilayers were prepared under each solvent test condition. The total QCM frequency change for a (dendrimer/PA-AgNP)$_5$ multilayer sample was measured after drying to calibrate the frequency (or mass) loss of the nine samples for a given bilayer number as a percent loss change in organic or aqueous media. The samples were subsequently immersed in an organic solvent or water bath for different dipping time periods (1, 5, 15, 35, 60, 90, 120, 180, and 240 min). The frequency changes of the dried samples were then plotted as a function of time.

Fourier Transform Infrared Spectroscopy (FTIR). Vibrational spectra were measured by FTIR spectroscopy (iS10 FT-IR, Thermo Fisher) in the transmission and attenuated total reflection (ATR) modes. The sample chamber was purged with N_2 gas for 2 h to eliminate water and CO_2 prior to conducting the FTIR measurement. An ATR-FTIR spectrum for the (dendrimer/hydrophobic NP)$_n$ film deposited onto a Au-coated substrate was obtained from 300 scans with an incident angle of 80°. The acquired raw data were plotted after baseline correction, and the spectrum was smoothed using spectrum analyzing software (OMNIC, Nicolet).

Fabrication of Resistive Switching Memory Devices. All of the samples were prepared on Si substrates (2 cm × 2 cm) with a SiO_2 layer of about 100 nm thickness. A Ti layer of 20 nm thickness was then deposited on the substrates, and 100 nm thick bottom electrode (Pt) was subsequently deposited using the DC-magnetron sputtering system. The (dendrimer/Fe_3O_4)$_3$ multilayer films were then formed on the Pt-coated Si substrates. The resistive switching memory properties of resultant multilayer films were measured using a tungsten electrode with

50 μm diameter without any additional thermal treatment. To investigate the resistive switching behavior of LbL multilayered devices, the current−voltage (I−V) curves were measured by a semiconductor parametric analyzer (SPA, Agilent 4155B) in air environment. The pulsed voltage duration dependence of high- and low-current states was investigated using a semiconductor parametric analyzer (HP 4155A) and pulse generator (Agilent 81104A). The electrical switching properties of about 50 samples were measured, and reasonable switching results were obtained in 60% of the samples in the laboratory environment.

Conflict of Interest: The authors declare no competing financial interest.

Acknowledgment. This work was supported by NRF grant funded by the Korea government (MEST) (2010-0029106; R11-2005-048-00000-0).

Supporting Information Available: A degree of relative conversion of AgNP ligands, UV−vis spectra of (dendrimer/hydrophobic NP)$_n$ multilayers, TGA data of dendrimer/PA-AgNP multilayers, AFM image of single dendrimer layer, magnetic curve of (dendrimer/OA-Fe_3O_4)$_7$ multilayer, HR-TEM image of aqueous anionic Fe_3O_4 NPs, I−V curves of multilayer devices. This material is available free of charge *via* the Internet at http://pubs.acs.org.

REFERENCES AND NOTES

1. Decher, G. Fuzzy Nanoassemblies: Toward Layered Polymeric Multicomposites. *Science* **1997**, *277*, 1232–1237.
2. Caruso, F.; Caruso, R. A.; Möhwald, H. Nanoengineering of Inorganic and Hybrid Sphere by Colloidal Templating. *Science* **1998**, *282*, 1111–1114.
3. Podsiadlo, P.; Kaushik, A. K.; Arruda, E. M.; Waas, A. M.; Shim, B. S.; Xu, J. D.; Nandivada, H.; Pumplin, B. G.; Lahann, J.; Ramamoorthy, A.; *et al.* Ultrastrong and Stiff Layered Polymer Nanocomposites. *Science* **2007**, *318*, 80–83.
4. Lee, S. W.; Kim, J.; Chen, S.; Hammond, P. T.; Shao-Horn, Y. Carbon Nanotube/Manganese Oxide Ultrathin Film Electrodes for Electrochemical Capacitors. *ACS Nano* **2010**, *4*, 3889–3896.
5. Yu, A.; Liang, Z.; Cho, J.; Caruso, F. Nanostructured Electrochemical Sensor Based on Dense Gold Nanoparticle Films. *Nano Lett.* **2003**, *3*, 1203–1207.
6. Jiang, C.; Markutsya, S.; Pikus, Y.; Tsukruk, V. V. Freely Suspended Nanocomposite Membranes as Highly Sensitive Sensors. *Nat. Mater.* **2004**, *3*, 721–728.
7. Lee, S.; Lee, B.; Kim, B. J.; Park, J.; Bae, W. K.; Char, K.; Hawker, C. J.; Bang, J.; Cho, J. Free-Standing Nanocomposite Multilayers with Various Length Scales, Adjustable Internal Structures, and Functionalities. *J. Am. Chem. Soc.* **2009**, *131*, 2579–2587.
8. Bae, W. K.; Kwak, J.; Lim, J.; Lee, D.; Nam, M. K.; Char, K.; Lee, C.; Lee, S. Multicolored Light-Emitting Diodes Based on All-Quantum-Dot Multilayer Films Using Layer-by-Layer Assembly Method. *Nano Lett.* **2010**, *10*, 2368–2373.
9. Lee, B.; Kim, Y.; Lee, S.; Kim, Y. S.; Wang, D.; Cho, J. Layer-by-Layer Growth of Polymer/Quantum Dot Composite Multilayers by Nucleophilic Substitution on Organic Media. *Angew. Chem., Int. Ed.* **2010**, *49*, 359–363.
10. Kim, Y.; Lee, C.; Shim, I.; Wang, D.; Cho, J. Nucleophilic Substitution Reaction Based Layer-by-Layer Growth of Superparamagnetic Nanocomposite Films with High Nonvolatile Memory Performance. *Adv. Mater.* **2010**, *22*, 5140–5144.
11. Lee, J.-S.; Cho, J.; Lee, C.; Kim, I.; Park, J.; Kim, Y.; Shin, H.; Lee, J.; Caruso, F. Layer-by-Layer Assembled Charge Trap Memory Devices with Adjustable Electronic Properties. *Nat. Nanotechnol.* **2007**, *2*, 790–795.
12. Tettey, K. E.; Yee, M. Q.; Lee, D. Photocatalytic and Conductive MWCNT/TiO_2 Nanocomposite Thin Films. *ACS Appl. Mater. Interfaces* **2010**, *2*, 2646–2652.
13. Tang, Z. Y.; Kotov, N. A.; Magonov, S.; Ozturk, B. Nanostructured Artificial Nacre. *Nat. Mater.* **2003**, *2*, 413–418.
14. Wang, T. C.; Cohen, R. E.; Rubner, M. F. Metallodielectric Photonic Structures Based on Polyelectrolyte Multilayers. *Adv. Mater.* **2002**, *14*, 1534–1537.
15. Zhao, N.; Shi, F.; Wang, Z.; Zhang, X. Combining Layer-by-Layer Assembly with Electrodeposition of Silver Aggregates for Fabricating Superhydrophobic Surfaces. *Langmuir* **2005**, *21*, 4713–4716.
16. Gao, M.; Sun, J.; Dulkeith, E.; Gaponik, N.; Lemmer, U.; Feldmann, J. Lateral Patterning of CdTe Nanocrystal Films by the Electric Field Directed Layer-by-Layer Assembly Method. *Langmuir* **2002**, *18*, 4098–4102.
17. Mamedov, A.; Ostrander, J.; Aliev, F.; Kotov, N. A. Stratified Assemblies of Magnetite Nanoparticles and Montomorillonite Prepared by the Layer-by-Layer Assembly. *Langmuir* **2000**, *16*, 3941–3949.
18. Lee, D.; Rubner, M. F.; Cohen, R. E. All-Nanoparticle Thin-Film Coatings. *Nano Lett.* **2006**, *6*, 2305–2312.
19. Goulet, P. J.; Dantos, D. S.; Alvarez-Puebla, R. A.; Oliveira, O. N.; Aroca, R. F. Surface-Enhanced Raman Scattering on Dendrimer/Metallic Nanoparticle Layer-by-Layer Film Substrates. *Langmuir* **2005**, *21*, 5576–5581.
20. Crespo-Biel, O.; Dordi, B.; Reinhoudt, D. N.; Huskens, J. Supramolecular Layer-by-Layer Assembly: Alternating Adsorptions of Guest- and Host-Functionalized Molecules and Particles Using Multivalent Supramolecular Interactions. *J. Am. Chem. Soc.* **2005**, *127*, 7594–7600.
21. Zhang, F.; Srinivasan, M. P. Miltilayered Gold-Nanoparticle/Polyimide Composite Thin Film through Layer-by-Layer Assembly. *Langmuir* **2007**, *23*, 10102–10108.
22. Krasteva, N.; Besnard, I.; Guse, B.; Bauer, R. E.; Mullen, K.; Yasuda, A.; Vossmeyer, T. Self-Assembled Gold Nanoparticle/Dendrimer Composite Films for Vapor Sensing Applications. *Nano Lett.* **2002**, *2*, 551–555.
23. Joseph, Y.; Krasteva, N.; Besnard, I.; Guse, B.; Rosenberger, M.; Wild, U.; Knop-Gericke, A.; Schlogl, R.; Krustev, R.; Yasuda, A.; *et al.* Gold-Nanoparticle/Organic Linker Films: Self-Assembly, Electronic and Structural Characterisation, Composition and Vapour Sensitivity. *Faraday Discuss.* **2004**, *125*, 77–97.
24. Kotov, N. A.; Dékány, I.; Fendler, J. H. Layer-by-Layer Self-Assembly of Polyelectrolyte-Semiconductor Nanoparticle Composite Films. *J. Phys. Chem.* **1995**, *99*, 13065–13069.
25. Fendler, J. H. Self-Assembled Nanostructured Materials. *Chem. Mater.* **1996**, *8*, 1616–1624.
26. Cassagneau, T.; Mallouk, T. E.; Fendler, J. H. Layer-by-Layer Assembly of Thin Film Zener Diodes from Conducting Polymers and CdSe Nanoparticles. *J. Am. Chem. Soc.* **1998**, *120*, 7848–7859.
27. Park, J.; An, K.; Hwang, Y.; Park, J.-G.; Noh, H.-J.; Kim, J.-Y.; Park, J.-H.; Hwang, N.-M.; Hyeon, T. Ultra-Large-Scale Syntheses of Monodisperse Nanocrystals. *Nat. Mater.* **2004**, *3*, 891–895.
28. Bruchez, M.; Moronne, M.; Gin, P.; Alivisatos, A. P. Semiconductor Nanocrystals as Fluorescent Biological Labels. *Science* **1998**, *281*, 2013–2016.
29. Chan, W. C. W.; Nie, S. Quantum Dot Bioconjugates for Ultrasensitive Nonisotopic Detection. *Science* **1998**, *281*, 2016–2018.
30. Gittins, D. I.; Susha, A. S.; Schoeler, B.; Caruso, F. Dense Nanoparticulate Thin Films *via* Gold Nanoparticle Self-Assembly. *Adv. Mater.* **2002**, *14*, 508–512.
31. Cho, J.; Char, K.; Hong, J.-D.; Lee, K.-B. Fabrication of Highly Ordered Multilayer Films Using Spin Self-Assembly Method. *Adv. Mater.* **2001**, *13*, 1076–1078.
32. Yoon, M.; Kim, Y.; Cho, J. Multifunctional Colloids with Optical, Magnetic, and Superhydrophobic Properties Derived from Nucleophilic Substitution-Induced Layer-by-Layer Assembly in Organic Media. *ACS Nano* **2011**, *5*, 5417–5426.
33. Grabar, K. C.; Allison, K. J.; Baker, B. E.; Bright, R. M.; Brown, K. R.; Freeman, R. G.; Fox, A. P.; Keating, C. D.; Musick, M. D.; Natan, M. J. Two-Dimensional Arrays of Colloidal Gold Particles: A Flexible Approach to Macroscopic Metal Surfaces. *Langmuir* **1996**, *12*, 2353–2361.
34. Schmitt, J.; Decher, G.; Dressick, W. J.; Brandow, S. L.; Geer, R. E.; Shashidhar, R.; Calvert, J. M. Metal Nanoparticle/Polymer Superlattice Films: Fabrication and Control of Layer Structure. *Adv. Mater.* **1997**, *9*, 61–65.

35. Xi, Q.; Chen, X.; Evans, D. G.; Yang, W. Gold Nanoparticle-Embedded Porous Graphene Thin Films Fabricated *via* Layer-by-Layer Self-Assembly and Subsequent Thermal Annealing for Electrochemical Sensing. *Langmuir* **2012**, *28*, 9885–9892.
36. Tettey, K. E.; Yee, M. Q.; Lee, D. Layer-by-Layer Assembly of Charged Particles in Nonpolar Media. *Langmuir* **2010**, *26*, 9974–9980.
37. Huang, H.-C.; Zacharia, N. S. Polyelectrolyte Multilayers and Complexes To Modify Secondary Interactions in Ethylene-*co*-Methacrylic Acid Ionomers. *ACS Macro Lett.* **2012**, *1*, 209–212.
38. Piao, L.; Lee, K. H.; Kwon, W. J.; Kim, S.-H.; Yoon, S. The Simple and Facile Methods To Improve Dispersion Stability of Nanoparticles: Different Chain Length Alkylcarboxylate Mixtures. *J. Colloid Interface Sci.* **2009**, *334*, 208–211.
39. Sun, S. Recent Advances in Chemical Synthesis, Self-Assembly, and Applications of FePt Nanoparticles. *Adv. Mater.* **2006**, *18*, 393–403.
40. Bellami, L. J. *The Infrared Spectra of Complex Molecules*; Wiley: New York, 1975; pp 123−126.
41. Nakamoto, K. *Infrared and Raman Spectra of Inorganic and Coordination Compounds*; Wiley: New York, 2008; pp 213−217.
42. Bernal, J. D.; Mason, J. Packing of Spheres: Co-ordination of Randomly Packed Spheres. *Nature* **1960**, *188*, 910–911.
43. Scott, G. D.; Kilgour, D. M. The Density of Random Close Packing of Spheres. *J. Phys. D* **1969**, *2*, 863–866.
44. Berryman, J. D. Random Close Packing of Hard Spheres and Disks. *Phys. Rev. A* **1983**, *27*, 1053–1061.
45. Tsukruk, V. V.; Rinderspacher, F.; Bliznyuk, V. N. Self-Self-Assembled Multilayer Films from Dendrimers. *Langmuir* **1997**, *13*, 2171–2176.
46. Sun, S.; Zeng, H.; Robinson, D. B.; Raoux, S.; Rice, P. M.; Wang, S. X.; Li, G. Monodisperse MFe_2O_4 (M-Fe, Co, Mn) Nanoparticles. *J. Am. Chem. Soc.* **2004**, *126*, 273–279.
47. Brust, M.; Bethell, D.; Schiffrin, D. J.; Kiely, C. J. Novel Gold-Dithiol Nano-Networks with Non-metallic Electronic Properties. *Adv. Mater.* **1995**, *7*, 795–797.
48. Gittins, D. I.; Caruso, F. Spontaneous Phase Transfer of Nanoparticulate Metals from Organic to Aqueous Media. *Angew. Chem., Int. Ed.* **2001**, *40*, 3001–3004.
49. Cho, J.; Caruso, F. Investigation of the Interactions between Ligand-Stabilized Gold Nanoparticles and Polyelectrolyte Multilayer Films. *Chem. Mater.* **2005**, *17*, 4547–4553.
50. Kim, K.; Lee, J. W.; Choi, J.-Y.; Shin, K. S. pH Effect on Surface Potential of Polyelectrolytes-Capped Gold Nanoparticles Probed by Surface-Enhanced Raman Scattering. *Langmuir* **2010**, *26*, 19163–19169.
51. Davis, S. C.; Klabunde, K. J. Unsupported Small Metal Particles: Preparation, Reactivity, and Characterization. *Chem. Rev.* **1982**, *82*, 153–208.
52. Jana, S.; Pande, S.; Sinha, A. K.; Pal, T. Synthesis of Superparamagnetic β-MnO_2 Organosol: A Photocatalyst for the Oxidative Phenol Coupling Reaction. *Inorg. Chem.* **2008**, *47*, 5558–5560.
53. Cai, Q. J.; Gan, Y.; Chan-Park, M. B.; Yang, H. B.; Lu, Z. S.; Li, C. M.; Guo, J.; Dong, Z. L. Solution-Processable Barium Titanate and Strontium Titanate Nanoparticle Dielectrics for Low-Voltage Organic Thin-Film Transistors. *Chem. Mater.* **2009**, *21*, 3153–3161.
54. Choi, J.; Rubner, M. F. Influence of the Degree of Ionization on Weak Polyelectrolyte Multilayer Assembly. *Macromolecules* **2005**, *38*, 116–124.
55. Waser, R.; Aono, M. Nanoionics-Based Resistive Switching Memories. *Nat. Mater.* **2007**, *6*, 833–840.
56. Strukov, D. B.; Snider, G. S.; Stewart, D. R.; Williams, R. S. The Missing Memristor Found. *Nature* **2008**, *453*, 80–83.
57. Yang, J. J.; Pickett, M. D.; Li, X.; Ohlberg, D. A. A.; Stewart, D. R.; Williams, R. S. Memrisitve Switching Mechanism for Metal/Oxide/Metal Nanodevices. *Nat. Nanotechnol.* **2008**, *3*, 429–433.
58. Baek, H.; Lee, C.; Park, J.; Kim, Y.; Koo, B.; Shin, H.; Wang, D.; Cho, J. Layer-by-Layer Assembled Enzyme Multilayers with Adjustable Memory Performance and Low Power Consumption *via* Molecular-Level Control. *J. Mater. Chem.* **2012**, *22*, 4645–4651.
59. Ko, Y.; Kim, Y.; Baek, H.; Cho, J. Electrically Bistable Properties of Layer-by-Layer Assembled Multilayers Based on Protein Nanoparticles. *ACS Nano* **2011**, *5*, 9918–9926.
60. Koo, B.; Baek, H.; Cho, J. Control over Memory Performance of Layer-by-Layer Assembled Metal Phthalocyanine Multilayers *via* Molecular-Level Manipulation. *Chem. Mater.* **2012**, *24*, 1091–1099.
61. Guan, W.; Long, S.; Jia, R.; Liu, M. Nonvolatile Resistive Switching Memory Utilizing Gold Nanocrystals Embedded in Zirconium Oxide. *Appl. Phys. Lett.* **2007**, *91*, 062111.
62. Mamedov, A.; Ostrander, J.; Aliev, F.; Kotov, N. A. Stratified Assemblies of Magnetite Nanoparticles and Montmorillonite Prepared by the Layer-by-Layer Assembly. *Langmuir* **2000**, *16*, 3941–3949.
63. Kim, T. H.; Jang, E. Y.; Lee, N. J.; Choi, D. J.; Lee, K.-J.; Jang, J.-T.; Choi, J.-S.; Moon, S. H.; Cheon, J. Nanoparticle Assemblies as Memristors. *Nano Lett.* **2009**, *9*, 2229–2233.
64. Shih, A.; Zhou, W.; Qiu, J.; Yang, H.-J.; Chen, S.; Mi, Z.; Shih, I. Highly Stable Resistive Switching on Monocrystalline ZnO. *Nanotechnology* **2010**, *21*, 125201.